EUROPEAN ORGANIZATION FOR NUCLEAR RESEARCH

CERN – AB DEPARTMENT

AB-Note-2005-033 OP
CARE/HIPPI-Document-2005-005

Design and Construction of a Beam Shape and Halo Monitor for the CERN SPL

K.Hanke, M.Hori

Abstract

We describe the design of a beam shape and halo monitor developed in the frame of the CERN SPL/Linac 4 study. The device is designed such that it can be used both for monitoring the correct functioning of the beam chopper and for transverse diagnostics of the H^- beam. Both applications require a dynamic range of the order of 10^6. We discuss the design choices that have been made and report on tests of the various detector components.

Geneva, Switzerland

2nd August 2005

1 Introduction

The CERN SPL (Superconducting Proton Linac)/Linac 4 design features a chopper structure at a beam energy of 3 MeV [1, 2]. The beam macro-pulse before chopping is bunched at 352 MHz, i.e. the bunch spacing is 2.84 ns. Each single bunch is populated with 4×10^8 H^- ions, with a bunch length of 0.5 ns. The chopper removes 3 out of 8 bunches, leaving five bunches in a row followed by three empty buckets. The correct functioning of the chopper is essential, as any remaining beam current in a chopped bucket may cause beam loss and contribute to the activation of components. Based on an acceptable beam loss of 1 W/m, we conclude that a maximum of 10^3 particles are acceptable in a chopped bucket. We require hence a device to measure the beam current in a chopped or partially chopped bucket down to an intensity of 10^3 particles, in the vicinity (2.84 ns) of a fully populated bunch. The required dynamic range is hence of the order of 10^6.

A further issue of high-intensity H^- linacs is halo formation. Particles expelled from the beam core can form a beam halo which can cause harmful beam loss at higher energy. Also in the case of beam halo, a number of 10^3 particles appears to be the upper acceptable limit. We therefore require a beam monitor capable of measuring the transverse beam halo down to 10^3 particles, and at the same time the beam core populated with several 10^8 particles. The halo particles are found at a radius of up to 2 cm and the beam core has a radius of the order of 0.5 cm. The active surface of the detector should hence be at least 4×4 cm, and the required dynamic range is again of the order of 10^6.

2 Comparison of Different Detector Designs

We have studied different detector types based on the emission and imaging of secondary electrons. These electrons can be generated by inserting a thin carbon foil into the beam. Measurements have to be performed with a shortened beam macro-pulse length ("diagnostic beam"), as a beam with nominal parameters would destroy the target. The method is destructive, as the beam is intercepted during a measurement. Alternatively, the electrons used for diagnostics can be detached from the H^- ions using a pulsed laser (non-destructive for most of the H^- ions). In all cases studied, electrons are used for longitudinal and transverse imaging of the H^- beam. We have studied in detail four possible technical approaches to this problem.

1. **Micro-channel plate (MCP) with segmented anode:** In this design, the H^- beam strikes a thin carbon foil, thus producing secondary electrons which are accelerated to a micro-channel plate (MCP) and multiplied by a factor of $\sim 10^3$–10^6 [3, 4, 5, 6, 7, 8]. The spatial beam profile is obtained by collecting the electrons on a series of segmented electrodes. Although the detector has the highest timing resolution (up to ~ 100 ps) and sensitivity (it can detect a single electron with 20–50% efficiency) among all the designs studied here, it had the following disadvantages, i): the MCPs we tested had low linearity (typically around 10–100, depending on the gain) and saturated at high beam intensities, ii): it is difficult to manufacture and read out segmented electrodes with the high position resolution (< 0.2 mm), large active area (40x40 mm), fast timing resolution (< 1 ns), and large number of channels (~ 50000) required here.
2. **p-i-n semiconductor diode or CMOS detectors:** Here the secondary electrons emitted from the above carbon foil are accelerated to an energy of 25 keV and strike an array of $p-i-n$ diode or CMOS "pixel" detectors [9, 10]. Each secondary electron produces ~ 1000 electron-hole pairs in the diode, and the resulting charge signal is measured by a readout chip bonded onto the back side of the detector. Although these semiconductor detectors have greatly advanced in recent years, we did not use them in the present application because i): a custom detector would have to be designed and manufactured using expensive photo-lithographic and ion implantation processes, even though we need only 2–3 such detectors, ii): the timing resolution of the detector is too low, being typically 5–50 ns depending on its capacitance and shaping time of its readout amplifiers, iii): the entrance window of the pixel detector must be made extremely thin (< 50 nm) to allow the passage of the low energy (10–25 keV) electrons; on the other hand, we require a robust detector which will not degrade after being repeatedly evacuated and exposed to air.
3. **Thermo-electrically cooled CCD detector with gatable phosphor screen and fiber optic bundle:** In this design, the electrons emitted by the foil are accelerated to an energy of ~ 6 keV and strike a phosphor screen [11], thereby producing scintillation light. The light propagates along a fiber optic bundle and is imaged by a charged coupled device (CCD) with spatial resolution $\Delta x \sim 20\mu$m and active area of 27 mm× 26 mm. A

time resolution of $\Delta t < 1$ ns is attained by applying high-voltage pulses of sub-nanosecond scale duration on a series of micro-wire mesh electrodes, which control the flow of secondary electrons from the foil to the phosphor screen. The CCD has a dynamic range of $\sim 10^4$, which can be further increased by varying the exposure time. The disadvantage of the detector is that it operates on the relatively complicated principle of first converting the secondary electrons into scintillation light, and then imaging the light with a CCD. Due to the low conversion efficiency involved in this extra step, the detector has the lowest sensitivity among all the designs described here.

4. **Laser photo-ionization detectors:** Here the H^- beam is irradiated by a pulsed laser beam of power density ~ 1 MW/cm^2. The ions are photo-ionized in the strong laser field, and the emerging electrons are collected by a Faraday cup or MCP detector [12, 13]. The profile of the H^- beam is measured by focusing the laser beam to e.g. a ~ 100 μm-diameter spot, and scanning it along the spatial distribution of the H^- beam. While the other detectors described here are destructive (i.e. they intercept and degrade all of the H^- beam during spatial measurements), the laser ionization detector has the advantage of being non-destructive (i.e. only a small portion of the H^- ions comprising the beam would be ionized, while most of them would pass through the detector without any degradation). Moreover, by adjusting the pulse length of the ionizing laser, timing resolutions of < 10 ps are theoretically possible. One of the authors (M. Hori) is developing a similar apparatus for detecting the spatial distribution of certain types of gases using a Nd:YAG laser of wavelength $\lambda = 213$–532 nm.

3 Design and Construction of the Detector

We have chosen the third design above (thermo-electrically cooled CCD detector with gatable phosphor screen and fiber optic bundle) because it satisfied the requirements concerning the high dynamic range, spatial resolution, and sub-nanosecond-scale timing response. The detector was developed during the years 2002–2005. This included the study of various techniques to increase its sensitivity. In the following section we describe tests of the various detector components that have been performed.

The detector was housed in a 20 cm$\times$ 50 cm$\times$ 50 cm vacuum chamber made of type 316LN non-magnetic stainless steel. It was important to keep the total length of the detector along the beam path as short as possible ($l < 20$ cm), so that any adiabatic increase in the emittance of the beam traveling through the detector would be minimized. A carbon foil of size 60 mm$\times$ 50 mm and thickness $t_d = 10 - 50$ μg/cm^2 was suspended in the center of the chamber at a 45-degree angle with respect to the H^- beam. The foil was mounted on a stainless steel electrode measuring 20 cm$\times$ 18 cm, which was insulated using a series of ceramic spacers and biased between $V = -1$ and -5 kV. Two types of foils were used, i): amorphous carbon foils made by evaporating carbon onto a plastic foil in vacuum, ii): carbon foils made by modified controlled ACDC arc discharge (mCADAD), which have lifetimes several times longer than those produced by evaporation.

A stack of four micro-wire grids was positioned parallel to the carbon foil, at a distance $l \sim 60$ mm from it. Each grid consisted of 30 gold-coated tungsten wires of diameter 10 μm and pitch 2 mm, stretched over a ceramic frame with a 50 mm $\times$ 50 mm rectangular hole in the center to allow the passage of secondary electrons. Pulse voltages of amplitude $V = 0.5$–6 kV, rise time < 1 ns, and pulse-lengths $\Delta t = 10$–100 ns were applied to the grids, thus producing an uniform electric field between the carbon foil and grids which accelerated the electrons. By adjusting the timing of these pulsed voltages, the detector could be rapidly turned on and off, thus allowing it to probe various time slices along the temporal profile of the H^- beam. The pulsed voltages were produced either by avalanche transistors or field effect transistors. In order to apply potentials with 1-ns-scale rise times on the grids, each grid was connected in parallel to a set of four high-voltage pulsars by coaxial cables of impedance $50\ \Omega$, thus achieving an effective impedance $12\ \Omega$.

The secondary electrons accelerated by the grids are impinged on a phosphor screen; this screen was manufactured by first depositing a thin layer of indium tin oxide (produced by Proxitronic GmbH) on the surface of a 50 mm$\times$50 mm$\times$ 3 mm fiber optic plate. Type P47 ($Y_2SiO_5 : Ce, Tb$) phosphor grains of 1-μm size were then deposited, followed by evaporation of a 40-nm-thick aluminum layer. This phosphor emitted scintillation light at wavelength ~ 370–480 nm with a short lifetime of ~ 100 ns, which was needed to obtain a high time resolution.

The aluminum layer served for three purposes, i): only those electrons accelerated to energies of more than a few keV could penetrate the layer and produce scintillation light, whereas lower energy electrons were stopped by it. The detector could thus be quickly turned on or off by adjusting the incident energy of secondary electrons, ii): it prevented stray light or the glow from the carbon foil heated by the H^- beam from entering the fiber optic bundle, iii): it reflected part of the scintillation light emitted from the phosphor layer into the fiber optic plate, thus increasing the light collection efficiency by a factor of ~ 2.

The image of the scintillation light was transmitted along a 130 mm long, $d = 60$ mm diameter conduit attached to the back side of the phosphor screen. The conduit consisted of $10\ \mu$m diameter optical fibers bundled together, and tapered off to a diameter $d = 40$ mm at its end; thus any image transmitted through the conduit was unmagnified by a factor of 1.5. The exit side of the conduit was connected to a 26.8 mm $\times$ 26.0 mm CCD sensor (Princeton Instruments SCX-1300) with a pixel resolution of $20\ \mu$m. The sensor had quantum efficiencies between 0 and $\sim 15\%$ at the emission wavelengths of the P47 phosphor. The efficiency of detecting secondary electrons can be further increased by two orders of magnitude by using a type P43 phosphor screen, but we did not use this here because of its much longer ($\sim$ 1 ms) decay time. We tested the spatial resolution and image distortion of the detector by placing on the entrance surface of the fiber optic conduit a glass photo-mask with a pattern of grids. The spatial resolution was found to be better than 50μm, and any deformation along the entire aperture of the conduit was within a few percent.

The image acquired by the CCD was processed and recorded on a workstation running the Linux operating system and Labview software. The software enabled the detector to subtract any background noise and integrate over several CCD images, thus increasing the effective sensitivity and dynamic range. All images were remotely accessible from several workstations by broadcasting the data over the Ethernet network.

All subcomponents have by now been assembled on the vacuum chamber of the beam monitor. We plan to carry out the first tests of the complete detector by August 2005 using an ultraviolet pulsed Nd:YAG laser to simulate the H^- beam. The possibility of performing a particle beam test is currently being investigated.

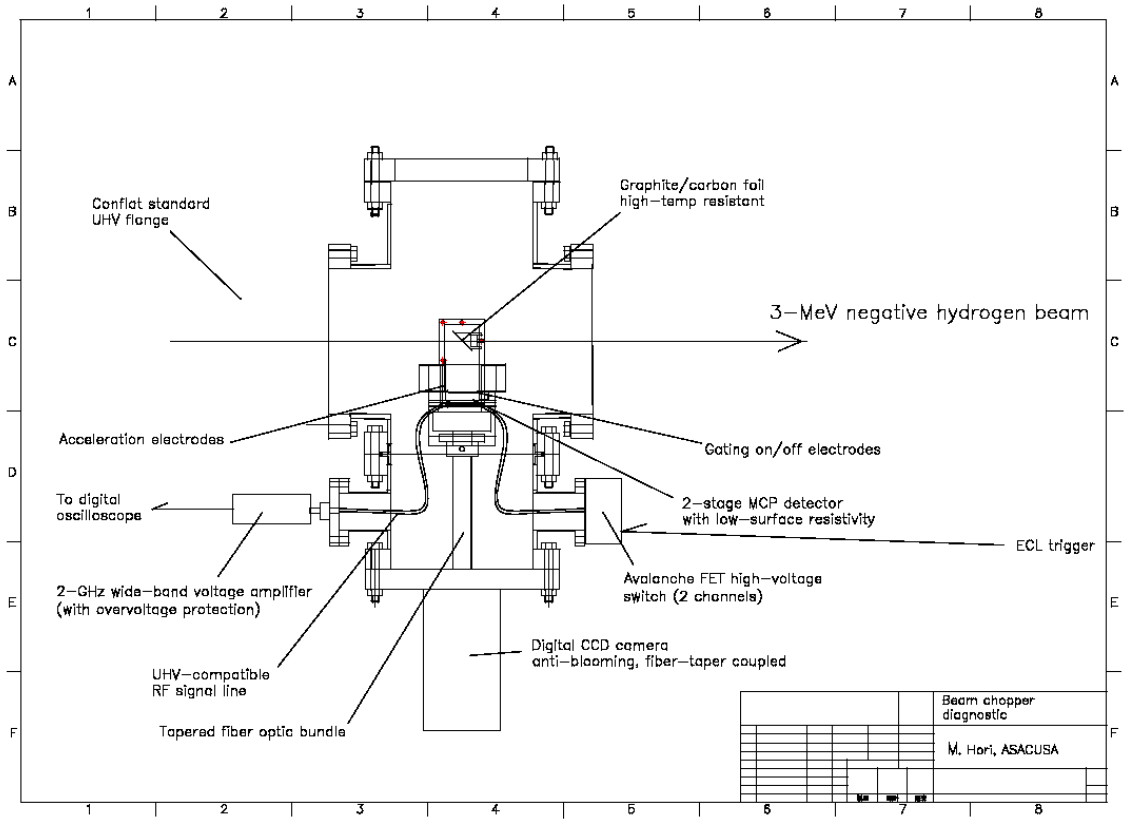

Figure 1: Side view of the beam shape and halo monitor. The system of target, secondary electron collection and gating is housed in a dedicated vacuum chamber. The dimension of the monitor in longitudinal direction is only 20 cm, as the set-up of the chopper beam line is very compact for beam dynamics reasons.

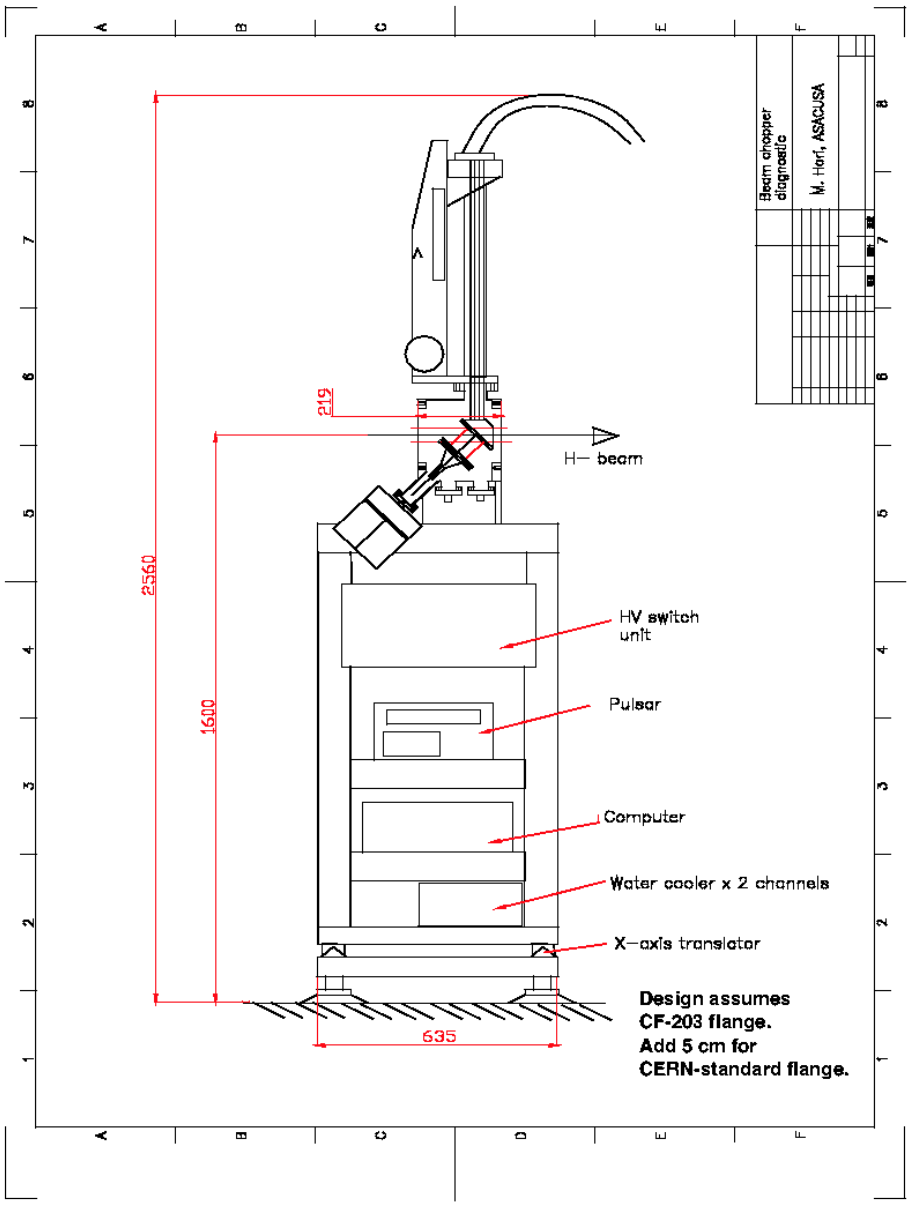

Figure 2: Overall side view of the monitor with foil actuator and support stand.

References

[1] R. Garoby, K. Hanke, A. Lombardi, C. Rossi, M. Vretenar, F. Gerigk, *Design of LINAC4, A New Injector for the CERN Booster*, conf. proc. LINAC2004 and CERN AB Note 2004-104 (2004).

[2] C. Rossi, L. Bruno, F. Caspers, R. Garoby, J. Genest, K. Hanke, M. Hori, D. Küchler, A. Lombardi, M. Magistris, A. Millich, M. Paoluzzi, E. Sargsyan, M. Silari, T. Steiner, M. Vretenar, P.-Y. Beauvais, P. Ausset, *The SPL Front-End: A 3 MeV H^- Test Stand at CERN*, conf. proc. LINAC2004 and CERN AB Note 2004-102 (2004).

[3] J.L. Culhane, Nucl. Instr. and Meth. **225** (1984) 51.

[4] S.H.W. Sigmund, M. Lampton, R. Raffant, W. Merrick, Nucl. Instr. and Meth. **310** (1991) 311.

[5] A.N. James, T.P. Morrison, K.L. Ying, K.A. Connell, H.G. Price, J. Simpson, Nucl. Instr. and Meth. A **267** (1988) 144.

[6] O.H. Odland, W. Mittig, A. Lepine-Szily, G. Fremont, M. Chartier, M. MacCormick, J.M. Casndjian, Nucl. Instr. and Meth. A **378** (1996) 149.

[7] D. Shapira, T.A. Lewis, L.D. Hulett Jr., Z. Ciao, Nucl. Instr. and Meth. Phys. Research A **449** (2000) 396.

[8] D. Shapira, T.A. Lewis, L.D. Hulett, Nucl. Instr. and Meth. Phys. Research A **454** (2000) 409.

[9] A.R. Faruqi, D.M. Cattermole, C. Raeburn, Nucl. Instr. and Meth. Phys. Research A **513** (2003) 317.

[10] W. Dulinski, A. Braem, M. Caccia, G. Claus, G. Deptuch, D. Grandjean, C. Joram, J.Séguinot, M. Winter, Nucl. Instr. and Meth. Phys. Research A **546** (2005) 274.

[11] J.P. Moy, A. Koch, and M.B. Nielsen, Nucl. Instr. and Meth. Phys. Research A **326** (1993) 581.

[12] R.C. Connolly, K.F. Johnson, D.P. Sandoval, V. Yuan, Nucl. Instr. and Meth. A **132** (1992) 415.

[13] V.W. Yuan, R.C. Connolly, R.C. Garcia, K.F. Johnson, K. Saadatmand, O.R. Sander, D.P. Sandoval, M.A. Shinas, Nucl. Instr. and Meth. A **329** (1993) 381.